

# Complete phase diagram of the spin- $\frac{1}{2}$ $J_1$ - $J_2$ - $J_3$ model (with $J_3 = J_2$ ) on the honeycomb lattice

P. H. Y. Li and R. F. Bishop

*School of Physics and Astronomy, The University of Manchester, Manchester, M13 9PL, UK*

We use the coupled cluster method to investigate the ground-state (GS) properties of the frustrated spin- $\frac{1}{2}$   $J_1$ - $J_2$ - $J_3$  model on the honeycomb lattice, with nearest-neighbor exchange coupling  $J_1$  plus next-nearest-neighbor ( $J_2$ ) and next-next-nearest-neighbor ( $J_3$ ) exchanges of equal strength. In particular we find a direct first-order phase transition between the Néel-ordered antiferromagnetic phase and the ferromagnetic phase at a value  $J_2/J_1 = -1.17 \pm 0.01$  when  $J_1 > 0$ , compared to the corresponding classical value of  $-1$ . We find no evidence for any intermediate phase. From this and our previous CCM studies of the model we present its full zero-temperature GS phase diagram.

PACS numbers: 75.10.Jm, 75.40.-s, 75.50.Ee

## I. INTRODUCTION

Frustrated quantum spin systems on regular two-dimensional (2D) lattices have been the subject of intense interest in recent years.<sup>1-3</sup> They exhibit a wide variety of different types of ordering and phases, even at zero temperature ( $T = 0$ ). Examples include various quasiclassical antiferromagnetic (AFM) phases (e.g., with Néel or columnar striped ordering), phases with quantum spiral ordering, valence-bond crystalline phases with nematic ordering, and spin-liquid phases. Of particular interest are the ( $T = 0$ ) quantum phase transitions that can occur as the coupling constants in the Hamiltonian are varied, so that the degree of frustration between bonds competing for various types of order is changed. The resulting interplay between magnetic frustration and quantum fluctuations has been seen to be a very effective means to create (and destroy) new types of order not present in the classical counterparts of the models. The successful syntheses of ever more quasi-2D magnetic materials, and the experimental investigation of their properties, has also served to intensify their theoretical study. The very recent prospects of being able to realise spin-lattice models with ultracold atoms trapped in optical lattices<sup>4</sup> is likely to make even more data available about the quantum phase transitions in the models as the exciting possibility opens up in such trapped-atom experiments to tune the strengths of the competing magnetic bonds, and hence to drive the system from one phase to another.

Since quantum fluctuations tend to be largest for the smallest values of the spin quantum number  $s$ , for lower dimensionality  $D$  of the lattice, and for the smallest coordination number  $z$  of the lattice, spin- $\frac{1}{2}$  models on the (hexagonal or) honeycomb lattice play a special role for  $D = 2$ , since the honeycomb lattice has the lowest  $z$  ( $= 3$ ) of all regular 2D lattices. Thus, for example, one of the few exactly solvable models on the honeycomb lattice, namely the Kitaev model,<sup>5</sup> has been shown to sustain a spin-liquid phase. Clearly, the honeycomb lattice is also relevant to the study of graphene, for which much of the physics may be describable in terms of Hubbard-like models on this lattice.<sup>6</sup> Evidence

has also been found from quantum Monte Carlo (QMC) studies<sup>7</sup> that quantum fluctuations are sufficiently strong to establish an insulating spin-liquid phase between the nonmagnetic metallic phase and the antiferromagnetic (AFM) Mott insulator phase, when the Coulomb repulsion parameter  $U$  becomes moderately strong. For large values of  $U$  the latter phase corresponds to the pure Heisenberg antiferromagnet (HAFM) on the bipartite honeycomb lattice, whose GS phase exhibits Néel LRO. However, higher-order terms in the  $t/U$  expansion of the Hubbard model may lead to frustrating exchange couplings in the corresponding spin-lattice limiting model, in which the HAFM with nearest-neighbor (NN) exchange couplings is the leading term in the large- $U$  expansion. Frustration is easily incorporated via competing next-nearest-neighbor (NNN) and maybe also next-next-nearest-neighbor (NNNN) bonds. Recent calculations of the low-dimensional material  $\beta$ -Cu<sub>2</sub>V<sub>2</sub>O<sub>7</sub> also show that its magnetic properties can be described in terms of a spin- $\frac{1}{2}$  model on a distorted honeycomb lattice.<sup>8</sup>

For all these and other reasons, frustrated spin- $\frac{1}{2}$  Heisenberg models on the honeycomb lattice, including couplings  $J_1$ ,  $J_2$ , and  $J_3$  up to third nearest neighbors, have been extensively studied using a variety of theoretical tools.<sup>9-21</sup> The Hamiltonian for the system is

$$H = J_1 \sum_{\langle i,j \rangle} \mathbf{s}_i \cdot \mathbf{s}_j + J_2 \sum_{\langle\langle i,k \rangle\rangle} \mathbf{s}_i \cdot \mathbf{s}_k + J_3 \sum_{\langle\langle\langle i,l \rangle\rangle\rangle} \mathbf{s}_i \cdot \mathbf{s}_l, \quad (1)$$

where  $i$  runs over all lattice sites on the lattice, and  $j$  runs over all NN sites,  $k$  over all NNN sites, and  $l$  over all NNNN sites to  $i$ , respectively, counting each bond once and once only. Each site  $i$  of the lattice carries a particle with spin operator  $\mathbf{s}_i$  and spin quantum number  $s = \frac{1}{2}$ . The lattice and the exchange bonds are illustrated in Fig. 1.

The solution of the classical version of the model (i.e., when  $s \rightarrow \infty$ ) is itself rich.<sup>9,10</sup> For the AFM version of the model (i.e., when  $J_1 > 0$ ) there are six different ground-state (GS) phases, comprising three different collinear AFM phases, the ferromagnetic (FM) state, and two different helical phases (and see, e.g., Fig. 2 of Ref. 10). The AFM phases are the Néel phase (N) shown in Fig. 1, and

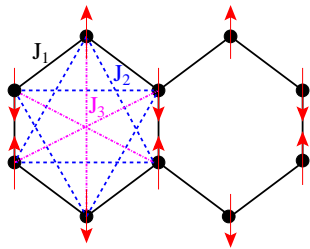


FIG. 1: (Color online) The Néel state and the bonds of the  $J_1$ - $J_2$ - $J_3$  honeycomb model; the arrows represent spins located on lattice sites  $\bullet$ .

the so-called striped (S) and anti-Néel (aN) phases. The S, aN, and N states have, respectively, 1, 2, and all 3 NN spins to a given spin antiparallel to it. Equivalently, if we consider the sites of the honeycomb lattice to form a set of parallel sawtooth (or zigzag) chains (in any one of the three equivalent directions), the S state comprises alternating FM chains, while the aN state comprises AFM chains in which NN spins on adjacent chains are parallel. There are actually infinite manifolds of non-coplanar states degenerate in energy with each of the S and aN states at  $T = 0$ , but both thermal and quantum fluctuations select the collinear configurations.<sup>10</sup> At the classical level there is an exact symmetry between the GS phase diagrams of the AFM ( $J_1 > 0$ ) and FM ( $J_1 < 0$ ) models, whereby one maps into the other under the interchanges  $J_1 \rightleftharpoons -J_1$ ,  $J_3 \rightleftharpoons -J_3$ , and  $\mathbf{s}_i \rightleftharpoons -\mathbf{s}_i$ , for sites  $i$  belonging to one of the two equivalent triangular sublattices of the honeycomb lattice (c.f., Figs. 2 and 3 of Ref. 10). When all three bonds are AFM in nature, the three possible GS phases (viz., the N, S, and one of the helical phases) meet at a tricritical point at  $J_3 = J_2 = J_1/2$ .

The line  $J_3 = J_2$  ( $\equiv \alpha J_1$ ) is thus of special interest, and we henceforth restrict ourselves to this situation where the NNN and NNNN bonds have equal strength for the remainder of the paper. There are then 4 GS classical phases. For the AFM case (with  $J_1 > 0$ ) we have: (a) the AFM S state when  $\alpha > \frac{1}{2}$ ; (b) the AFM N state when  $-1 < \alpha < \frac{1}{2}$ ; and (c) the FM state when  $\alpha < -1$ . For the FM case (with  $J_1 < 0$ ) we have: (a) the FM state when  $\alpha > -\frac{1}{10}$ ; (b) a spiral state when  $-\frac{1}{5} < \alpha < -\frac{1}{10}$ ; and (c) the AFM S state when  $\alpha < -\frac{1}{5}$ . The N state has classical first-order phase transitions to both the S state and the FM state, while the spiral state has continuous transitions to both the S state and the FM state.

In two previous papers<sup>15,20</sup> we have applied the coupled cluster method (CCM) to the  $s = \frac{1}{2}$  version of this model (with  $J_3 = J_2$ ). For the AFM case (with  $J_1 > 0$ ) we found<sup>15</sup> that the direct classical first-order phase transition between the two (N and S) AFM states at  $\alpha_{cl}^{N-S} = 0.5$  is changed for the quantum  $s = \frac{1}{2}$  model into two separate transitions, so that a Néel-ordered (N) phase exists for  $\alpha < \alpha_{c1} \approx 0.47$  and an AFM stripe-ordered (S) phase exists for  $\alpha > \alpha_{c2} \approx 0.60$ . In between, for  $\alpha_{c1} < \alpha < \alpha_{c2}$ , we found a paramagnetic GS phase

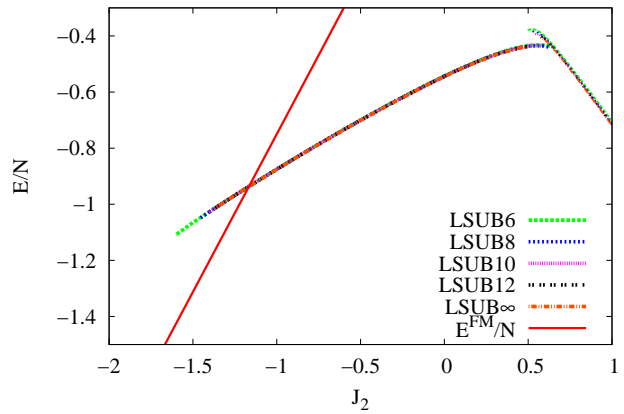


FIG. 2: (Color online) CCM LSUB $m$  results for the GS energy per spin,  $E/N$ , ( $J_1 \equiv 1$  and  $J_3 = J_2$ ) based on the Néel state (left thick curves) and striped state (right thin curves) as model states. We show calculated results for  $m = \{6, 8, 10, 12\}$  and the extrapolated LSUB $\infty$  result (see text). The exact FM result,  $E^{FM}/N = 3(1 + 3J_2)/8$ , is also shown.

with plaquette valence-bond crystalline (PVBC) ordering that has no classical counterpart. We further found that the quantum critical point (QCP) at  $\alpha_{c2}$  appears to be first order, while that at  $\alpha_{c1}$  is continuous. Since the N and PVBC phases break different symmetries we argued that our results favor the deconfinement scenario<sup>22</sup> for the latter transition. For the FM case (with  $J_1 < 0$ ) we found<sup>20</sup> that the two classical transitions from the spiral phase to the S phase at  $\alpha_{cl}^{sp-S} = -0.2$  and from the spiral phase to the FM phase at  $\alpha_{cl}^{sp-FM} = -0.1$  are changed for the quantum  $s = \frac{1}{2}$  model into one of two scenarios, namely, either a direct first-order transition between the the AFM S state and the FM state at  $\alpha_{c3} \approx -0.11$ , or there exists an intervening phase between them in the very narrow range  $-0.12 \lesssim \alpha \lesssim -0.10$ .

In order to complete the phase diagram of the spin- $\frac{1}{2}$  model there remains to investigate the quantum analog of the classical first-order transition at  $\alpha_{cl}^{N-FM} = -1$  between the AFM N state and the FM state for the AFM case (with  $J_1 > 0$ ), and that is the purpose of this paper. We shall again use the CCM to do so. The two states for the classical model have respective energies per spin given by  $E_{cl}^N/N = \frac{3}{2}s^2(-J_1 + J_2)$  and  $E_{cl}^{FM}/N = \frac{3}{2}s^2(J_1 + 3J_2)$ . Hence at the phase transition point  $\alpha_{cl}^{N-FM} = -1$  the GS energy per spin is  $E_{cl}/N = -\frac{3}{4}$  if we take  $s = \frac{1}{2}$  and  $J_1 = +1$  to set the energy scale. In all that follows we take  $J_1 \equiv 1$ .

The CCM (see, e.g., Refs. 23–25 and references cited therein) is one of the most powerful and most versatile modern techniques in quantum many-body theory. It has been applied to many quantum magnets with huge success (see Refs. 15,20,21,25–28 and references cited therein). The interested reader can find details of the

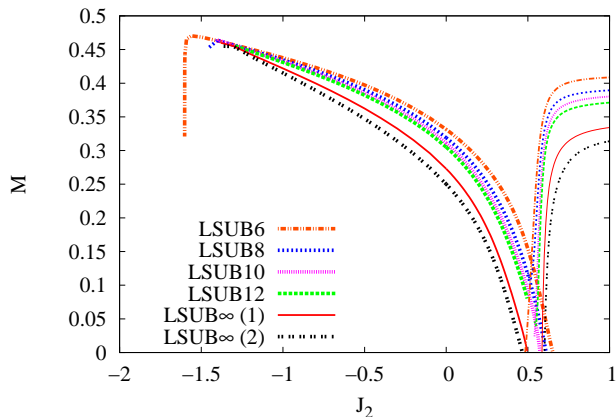


FIG. 3: (Color online) CCM LSUB $m$  results for the GS order parameter,  $M$ , ( $J_1 \equiv 1$  and  $J_3 = J_2$ ) based on the Néel state (left thick curves) and striped state (right thin curves) as model states. We show calculated results for  $m = \{6, 8, 10, 12\}$  and the extrapolated LSUB $\infty$ (1) and LSUB $\infty$ (2) results (see text).

CCM in the references cited, and we do not elaborate here. We note only that it is a size-extensive method that provides results from the outset in the infinite-lattice limit ( $N \rightarrow \infty$ ). The method requires us to provide a model (or reference) state, with respect to which the quantum correlations are expressed. Here we simply use the N state shown in Fig. 1, although for comparison purposes we also display below results obtained previously<sup>15</sup> based on the S state. As before, we use the well-tested localized lattice-animal-based subsystem (LSUB $m$ ) truncation scheme in which all multispin correlations are retained in the CCM correlation operators over all distinct locales on the lattice defined by  $m$  or fewer contiguous sites. The method of solving for higher orders of LSUB $m$  approximations is discussed in detail in Ref. 24.

The number of independent fundamental clusters increases rapidly with the LSUB $m$  truncation index  $m$ . Hence, it is essential to employ parallel processing techniques and supercomputing resources for larger values of  $m$ .<sup>29</sup> To obtain results in the (exact)  $m \rightarrow \infty$  limit, we need to extrapolate the raw LSUB $m$  data. Since the hexagon is a fundamental element of the honeycomb lattice we use LSUB $m$  data only with  $m \geq 6$ . For the GS energy per spin we employ the usual and well-tested scheme,  $E(m)/N = a_0 + a_1 m^{-2} + a_2 m^{-4}$ . For the magnetic order parameter (or average onsite magnetization),  $M$ , different schemes have been used for different situations. For models with no or only little frustration a well-tested scheme is  $M(m) = b_0 + b_1 m^{-1} + b_2 m^{-2}$ , whereas a more appropriate scheme for highly frustrated models, especially those showing a GS quantum phase transition, is  $M(m) = c_0 + c_1 m^{-1/2} + c_2 m^{-3/2}$ . We henceforth refer to these latter two schemes for  $M$  as LSUB $\infty$ (1) and LSUB $\infty$ (2), respectively. All of the the extrapolations shown below are based on LSUB $m$  results

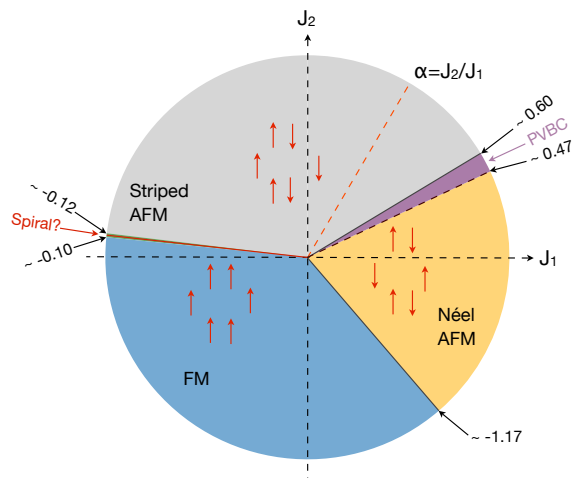


FIG. 4: (Color online) The phase diagram of the spin- $\frac{1}{2}$   $J_1$ - $J_2$ - $J_3$  honeycomb model in the  $J_1$ - $J_2$  plane, for the case  $J_3 = J_2$ . The continuous transition between the Néel and PVBC phases at  $J_2/J_1 \equiv \alpha = \alpha_{c_1} \approx 0.47$  is shown by a broken line, while the first-order transition between the PVBC and striped phases at  $\alpha_{c_2} \approx 0.60$  is shown by a solid line. The transition between the striped and FM phases is either a first-order one at  $\alpha_{c_3} \approx -0.11$ , shown by a solid line, or occurs via an intermediate phase, probably with noncollinear spiral order, which exists in the region  $-0.12 \lesssim \alpha \lesssim -0.10$ . The first-order transition between the FM and the Néel phases at  $\alpha_{c_4} \approx -1.17$  is shown by a solid line.

with  $m = \{6, 8, 10, 12\}$ .

## II. RESULTS

In Fig. 2 we show our CCM results for the GS energy per spin,  $E/N$ . They are evidently very well converged for all values of  $J_2$  shown. There is a clear energy crossing of the FM and (extrapolated) N energy curves at a value  $\alpha_{c_4} \approx -1.17$ , with  $E/N \approx -0.941$ , which is direct evidence of a first-order phase transition, just as in the classical case where it occurs at  $\alpha_{cl}^{N-FM} = -1$  with  $E_{cl}/N = -0.75$ .

We note that the individual LSUB $m$  energy curves based on the Néel model state terminate at some lower critical value,  $\alpha_t^{LSUBm}$  which itself depends on the index  $m$ . These termination points, below which no real solutions to the coupled CCM equations exist, are themselves a reflection of the actual QCP at  $\alpha_{c_4}$ . For example,  $\alpha_t^{LSUB12} \approx -1.38$ . In Fig. 3 we show the corresponding results for the GS magnetic order parameter,  $M$ . We observe that the behavior of  $M$  on the Néel side near the QCP at  $\alpha_{c_4}$  is quite smooth, with the only indication of the transition to the FM state being the downturn very near the  $\alpha_t^{LSUBm}$  termination points. This is in sharp contrast to the behavior at the other end near the QCP of the N state with the PVBC state at  $\alpha_{c_1}$  where

$M \rightarrow 0$ . Clearly the best estimate for  $\alpha_{c_1}$  comes from the  $\text{LSUB}\infty(2)$  extrapolation, whereas the best estimate for  $M$  at the pure honeycomb HAFM point (i.e., when  $J_3 = J_2 = 0$ ) comes from the  $\text{LSUB}\infty(1)$  extrapolation, which gives  $M = 0.272 \pm 0.002$ , in excellent agreement with the value  $M = 0.2677 \pm 0.0006$  from a QMC simulation of lattices up to size  $N = 2048$ .<sup>30</sup> Figure 3 also clearly shows the corresponding transition at  $\alpha_{c_3}$  between the S state and the PVBC state, where again  $M \rightarrow 0$  on the striped phase side.

### III. SUMMARY AND CONCLUSIONS

In this and previous papers,<sup>15,20</sup> we have studied the spin- $\frac{1}{2}$   $J_1$ - $J_2$ - $J_3$  Heisenberg model, with  $J_2 = J_3$ , on the honeycomb lattice, using the CCM. In the present paper we have concentrated on completing the phase diagram. In particular we find that the classical direct first-order phase transition for the AFM case (where  $J_1 > 0$ ) between the AFM Néel-ordered phase and the FM phase is preserved for the quantum spin- $\frac{1}{2}$  model, but now occurs

at a QCP,  $\alpha_{c_4} \approx -1.17 \pm 0.01$ , compared to the classical value  $\alpha_{c_1}^{\text{N-FM}} = -1$ . Thus quantum fluctuations act to stabilize the collinear AFM order at the expense of the FM order, to higher values of frustration than in the classical case, as has also been observed in the FM version of the spin- $\frac{1}{2}$   $J_1$ - $J_2$  model on the square lattice.<sup>31</sup> We find no evidence that quantum fluctuations permit an intervening state with no classical counterpart, unlike the case of the transition between the two (Néel-ordered and stripe-ordered) AFM states which occurs as a direct first-order phase transition at  $\alpha_{c_1}^{\text{N-S}} = 0.5$  for the classical model, but occurs in the quantum spin- $\frac{1}{2}$  model via the intermediate PVBC phase.

Our results from this and our previous CCM studies<sup>15,20</sup> are summarised in the complete phase diagram for the model shown in Fig. 4.

We thank the University of Minnesota Supercomputing Institute for Digital Simulation and Advanced Computation for the grant of supercomputing facilities. We also thank D. J. J. Farnell and J. Richter for fruitful discussions.

- 
- <sup>1</sup> U. Schollwöck, J. Richter, D. J. J. Farnell, and R. F. Bishop (eds.), *Quantum Magnetism*, Lecture Notes in Physics **645** (Springer-Verlag, Berlin, 2004).
- <sup>2</sup> H. T. Diep (ed.), *Frustrated Spin Systems*, (World Scientific, Singapore, 2005).
- <sup>3</sup> J. B. Parkinson and D. J. J. Farnell, *An Introduction to Quantum Spin Systems*, Lecture Notes in Physics **816** (Springer-Verlag, Berlin, 2010), Chap. 11.
- <sup>4</sup> J. Struck, C. Ölschäger, R. Le Targat, P. Soltan-Panahi, A. Eckardt, M. Lewenstein, P. Windpassinger, and K. Sengstock, *Science* **333**, 996 (2011).
- <sup>5</sup> A. Kitaev, *Ann. Phys. (N.Y.)* **321**, 2 (2006); G. Baskaran, S. Mandal, and R. Shankar, *Phys. Rev. Lett.* **98**, 247201 (2007); J. Chaloupka, G. Jackeli, and G. Khaliullin, *ibid.* **105**, 027204 (2010)
- <sup>6</sup> A. H. Castro Neto, F. Guinea, N. M. R. Peres, K. S. Novoselov, and A. K. Geim, *Rev. Mod. Phys.* **81**, 109 (2009).
- <sup>7</sup> Z. Y. Meng, T. C. Lang, S. Wessel, F. F. Assaad, and A. Muramatsu, *Nature (London)* **464**, 847 (2010).
- <sup>8</sup> A. A. Tsirlin, O. Janson, and H. Rosner, *Phys. Rev. B* **82**, 144416 (2010).
- <sup>9</sup> E. Rastelli, A. Tassi, and L. Reatto, *Physica B & C* **97**, 1 (1979).
- <sup>10</sup> J. B. Fouet, P. Sindzingre, and C. Lhuillier, *Eur. Phys. J. B* **20**, 241 (2001).
- <sup>11</sup> A. Mulder, R. Ganesh, L. Capriotti, and A. Paramekanti, *Phys. Rev. B* **81**, 214419 (2010).
- <sup>12</sup> D. C. Cabra, C. A. Lamas, and H. D. Rosales, *Phys. Rev. B* **83**, 094506 (2011).
- <sup>13</sup> R. Ganesh, D. N. Sheng, Y.-J. Kim, and A. Paramekanti, *Phys. Rev. B* **83**, 144414 (2011).
- <sup>14</sup> B. K. Clark, D. A. Abanin, and S. L. Sondhi, *Phys. Rev. Lett.* **107**, 087204 (2011).
- <sup>15</sup> D. J. J. Farnell, R. F. Bishop, P. H. Y. Li, J. Richter, and C. E. Campbell, *Phys. Rev. B* **84**, 012403 (2011).
- <sup>16</sup> J. Reuther, D. A. Abanin, and R. Thomale, *Phys. Rev. B* **84**, 014417 (2011).
- <sup>17</sup> A. F. Albuquerque, D. Schwandt, B. Hetényi, S. Capponi, M. Mambrini, and A. M. Läuchli, *Phys. Rev. B* **84**, 024406 (2011).
- <sup>18</sup> J. Oitmaa and R. R. P. Singh, *Phys. Rev. B* **84**, 094424 (2011).
- <sup>19</sup> H. Mosadeq, F. Shahbazi, and S. A. Jafari, *J. Phys.: Condens. Matter* **23**, 226006 (2011).
- <sup>20</sup> P. H. Y. Li, R. F. Bishop, D. J. J. Farnell, J. Richter, and C. E. Campbell, *Phys. Rev. B* **85**, 085115 (2012).
- <sup>21</sup> P. H. Y. Li, R. F. Bishop, D. J. J. Farnell, and C. E. Campbell, arXiv:1201.3512v1 [cond-mat.str-el] (2011).
- <sup>22</sup> T. Senthil, L. Balents, S. Sachdev, A. Vishwanath, and M. P. A. Fisher, *Phys. Rev. B* **70**, 144407 (2004).
- <sup>23</sup> R. F. Bishop, *Theor. Chim. Acta* **80**, 95 (1991).
- <sup>24</sup> C. Zeng, D. J. J. Farnell, and R. F. Bishop, *J. Stat. Phys.* **90**, 327 (1998).
- <sup>25</sup> D. J. J. Farnell and R. F. Bishop, in *Quantum Magnetism* (Ref. 1), p.307.
- <sup>26</sup> R. Darradi, J. Richter, and D. J. J. Farnell, *Phys. Rev. B* **72**, 104425 (2005).
- <sup>27</sup> R. F. Bishop, P. H. Y. Li, R. Darradi, and J. Richter, *J. Phys.: Condens. Matter* **20**, 255251 (2008).
- <sup>28</sup> R. F. Bishop, P. H. Y. Li, D. J. J. Farnell, and C. E. Campbell, *Phys. Rev. B* **79**, 174405 (2009).
- <sup>29</sup> We use the program package CCCM of D. J. J. Farnell and J. Schulenburg, see <http://www-e.uni-magdeburg.de/jschulen/ccm/index.html>.
- <sup>30</sup> E. V. Castro, N. M. R. Peres, K. S. D. Beach, and A. W. Sandvik, *Phys. Rev. B* **73**, 054422 (2006).
- <sup>31</sup> J. Richter, R. Darradi, J. Schulenburg, D. J. J. Farnell, and H. Rosner, *Phys. Rev. B* **81**, 174429 (2010).